Journal of Superconductivity and Novel Magnetism (2020) 33:253 257
https://doi.org/10.1007/s10948-019-05268-5

ORIGINAL PAPER

# Silicon: a Revenant Thermoelectric Material?

Mark Lee[1]

Received: 25 June 2019 / Accepted: 15 August 2019 / Published online: 26 August 2019


**Abstract**
Before entering the world of superconductivity, Ted Geballe, in the 1950s, investigated the thermoelectric (TE) properties of doped crystalline silicon. Ted's results indicated that Si has very poor thermoelectric properties, primarily because near room temperature most of the heat transport through Si is carried via phonons rather than electrons and holes. These findings ended the role of Si in TE technologies for a half-century. A decade ago, it was proposed that Si in nanowire form can have good TE properties owing to suppression of phonon heat transport by surface scattering. However, no TE device made of Si nanowires has shown useful performance characteristics. Here, we present work showing integrated circuit Si TE generators that can generate power per unit area per applied temperature difference that is competitive with the best existing TE technologies using more exotic TE materials. Our devices surpass previous Si TE work not by increasing silicon's intrinsic TE efficiency but by exploiting modern Si processing technology to fabricate a very large number of heat harvesters per unit area. While Ted's old work buried Si in the TE world, our results may resurrect it as a viable TE material.

**Keywords** Thermoelectrics · Silicon · Semiconductors

## 1 Introduction

In the mid-1950s, Ted Geballe, then at Bell Laboratories, and colleagues made the first reliable measurements of the thermal and thermoelectric (TE) properties of doped silicon crystals [1, 2]. They were among the first to study Si crystals of comparable quality to what is used in the Si industry today, so their results continue to be cited in modern research. The main conclusion derived from Ted et al.'s results is that doped Si has a TE figure-of-merit, $ZT = (S^2/\rho\kappa)T$, of order $10^{-3}$ to $10^{-2}$ near room temperature, depending on dopant concentration. Here, $S$ is the Seebeck coefficient, $\rho$ the electrical resistivity, $\kappa$ the thermal conductivity, and $T$ the absolute temperature. Because the efficiency of a TE device, whether a generator or refrigerator, increases monotonically with $ZT$ [3], TE applications require materials with much higher $ZT$ values. Ted et al. attributed this small value of $ZT$ to the high phonon thermal conductivity in Si near $T = 300$ K. Because phonons are not charged, heat transport via lattice vibrations does not contribute to the Seebeck coefficient and makes $\kappa$ nearly independent of doping density at concentrations $\lesssim 10^{19}$ cm$^{-3}$. Thus, largely as a consequence of Ted et al.'s results, Si fell out of favor for TE applications. In the last several decades, TE technology has been based on more exotic materials such as the $(Bi,Sb)_2(Se,Te)_3$ system where $ZT \approx 1$.

TE generators have found various niche applications as a "green" energy technology that converts wasted heat into useful electrical power. Large-scale TE generators are employed to harvest the heat produced by bulk sources such as automobile engines, nuclear decay of a radioactive material, and solar concentrators [4, 5]. More recently, microelectronic TE devices aimed at on-chip thermal harvesting, heat management, and microwatt power sources for integrated circuit (IC) electronics has gained interest [6–8]. However, exotic high $ZT$ materials cannot be used with modern Si-based IC electronics because they are incompatible with the standardized industrial Si-processing methods that form the backbone of microelectronic technology.

In 2008, the notion that Si is not a useful TE material was challenged by two groups [9, 10] who both reported that Si in nanowire (NW) form can have $ZT$ as high as 0.6 near 300 K. If true, this would make Si competitive with exotic high $ZT$ materials, at least in microelectronic applications. The physical mechanism underlying a larger $ZT$ in Si NWs is thought to be the enhancement of surface scattering when the material

✉ Mark Lee
marklee@utdallas.edu

[1] Department of Physics, University of Texas at Dallas, Richardson, TX 75080, USA

has a very high surface-to-volume ratio. Surface scattering in principal decreases both $\kappa$ and $\rho$, but it is expected to suppress the phonon contribution to $\kappa$ far more than it suppresses $\rho$ because a phonon's mean-free-path is much longer that a charge carrier's. A higher *ZT* then results. This effect should become apparent when the NW diameter becomes smaller than the phonon mean-free-path, 100 to 200 nm in Si [11], but remains larger than the electron/hole mean-free-path, typically < 10 nm in doped Si. Experimental [9] and computational [11–14] results support this picture.

Refs. [9, 10] measured *S*, $\rho$, and $\kappa$ on individual doped Si NWs at different temperatures but did not construct an actual TE generator or refrigerator device. Following their work, many other groups tried to design and fabricate TE generators using Si NW [15–18] or other nanostructured Si elements [19, 20] as the active TE material. Disappointingly, the TE generator characteristics and efficiencies they found imply values of *ZT* consistent with that of bulk Si, not with the results of Refs. [9, 10].

In many practical applications, a TE generator is intended to operate between hot and cold thermal reservoirs each having virtually a constant temperature $T_H$ and $T_C$ respectively. The heat flow through the TE generator is small enough to have negligible effect on the temperature of the two reservoirs. In such a situation, the TE efficiency is much less important than how much electrical power per unit cross-sectional area for heat flow a TE generator can produce from the temperature difference $\Delta T = T_H - T_C$. The maximum power $P_{max}$ a TE generator produces is proportional both to $(\Delta T)^2$ and to cross-sectional area *A* [3]. Thus, the characteristic of interest is the specific power generation capacity $\Gamma_P = P_{max}/[A\cdot(\Delta T)^2]$, rather than the efficiency. Unlike *ZT*, $\Gamma_P$ is a circuit characteristic that is not necessarily tied to intrinsic material properties. $\Gamma_P$ can be increased, for example, by using a large number of thermocouples per unit area, even if each thermopile has a low *ZT*, and by minimizing parasitic electrical and thermal impedances. The best $(Bi,Sb)_2(Te,Se)_3$ TE generators [8, 21] have $\Gamma_P$ in the range of 2 to 100 μW cm$^{-2}$ K$^{-2}$. So to be practically competitive with a high *ZT*-based TE technology, a Si TE generator should attain $\Gamma_P$ of order 10 μW cm$^{-2}$ K$^{-2}$. Up to the present time, the highest $\Gamma_P$ in a Si-based TE generator is from Ref. [15] which reports $\Gamma_P = 0.48$ μW cm$^{-2}$ K$^{-2}$, still over one order-of-magnitude too small to challenge $(Bi,Sb)_2(Te,Se)_3$-based TE devices.

## 2 Design and Performance of Integrated Circuit Silicon Thermoelectric Generators

We recently developed [22] a series of Si IC TE generators that have demonstrated $\Gamma_P$ values ranging from 2 to 29 μW cm$^{-2}$ K$^{-2}$, making them comparable to $(Bi,Sb)_2(Te,Se)_3$ technology on a power generation performance basis. Moreover, our Si TE generators were fabricated using a standard "65 nm node" industrial process line that normally makes conventional microelectronic circuits such as microprocessors, radios, and signal processors. Consequently, our Si IC TEGs can take advantage of modern Si processing technology so that they should be orders-of-magnitude better than $(Bi,Sb)_2(Te,Se)_3$ technology on a cost-per-watt-generated basis.

The thermopiles in our TE generators consisted of doped *n*-type and *p*-type Si nanostructured "blades" connected electrically in series to form thermocouples. The typical blade dimensions were 80-nm width × 750-nm long × 350-nm tall. Thus, the blade width but not the length is smaller than the phonon mean-free-path in Si near room temperature. A blade geometry, rather than a NW geometry, was used to comply with standard process design rules.

Figure 1 a is a simplified sketch (not to scale) of the side view cross-section of a typical *n*-*p* thermocouple pair forming part of a thermopile in a TE generator. An actual TE generator consisted of ~ 100 such thermocouples, with a total cross-sectional area *A* for heat to flow from top to bottom of 48 μm × 36 μm. One thermocouple is formed from a pair of 4-blade nanostructured Si groups. All *n*-blades are connected electrically in parallel, all *p*-blades are connected electrically in parallel, and the *n*- and *p*-sides are connected electrically in series. At the top a resistive heater with a calibrated temperature coefficient of resistance was used as both a heat source

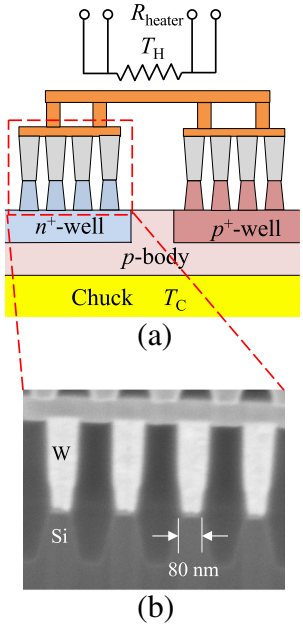


**Fig. 1** **a** Simplified illustration (not to scale) of the cross-section of a basic *n*-*p* thermocouple unit that forms a typical TE generator. A resistive heater supplies heat at temperature $T_H$ at the top, while the probe station chuck acts as a cold thermal reservoir at temperature $T_C$ at the bottom. The *n*- and *p*-type blades are typically grouped in sets of four, each blade contacted on top by a tungsten (*W*) plug. **b** SEM cross-section image of an actual 4-blade group forming one element of a thermocouple

and hot reservoir thermometer to set $T_H$, while the cold reservoir at the bottom is the copper probe station chuck with a calibrated thermometer embedded in the chuck that reads $T_C$. Thus, the *n*- and *p*-sides are connected thermally in parallel. Figure 1b is a scanning electron microscope cross-section image of an actual 4-blade group, showing the Si blades and the tungsten (*W*) electrical contacts.

Figure 2a shows thermopile current-voltage-power (*I-V-P*) data taken at several different $\Delta T$ on a representative TE generator. The TE power generated is $P = VI$. All devices showed a linear *I–V* with nearly constant slope. Increasing $\Delta T$ offsets the *I–V* line from the origin. The slope $R_S = |\Delta V/\Delta I|$ of the linear fit to the *I–V* data is the source resistance. At constant $\Delta T$, the open-circuit voltage, $V_{OC}$, and the short-circuit current, $I_{SC}$, are the intercepts of the *I–V* lines with the voltage and the current axes, respectively. The power generated $P = VI$ is thus a quadratic function of $I$ with maximum $P_{max} = \frac{1}{4}V_{OC}I_{SC} = (I_{SC})^2R_S/4$. $P_{max}$ is the power generated when the load resistance $R_L = R_S$, known as matched load conditions. Figure 2b shows that $P_{max}$ is a linear function of $(\Delta T)^2$, as expected. The slope of the fitted line in Fig. 2b is $1.41 \times 10^{-4}$ μW K$^{-2}$. Normalizing to the cross-sectional area $A$ then gives $\Gamma_P = P_{max}/[A\cdot(\Delta T)^2] =$ 8.2 μW cm$^{-2}$ K$^{-2}$ for this particular TE generator. Among all TE generator devices measured, $\Gamma_P$ ranged from 2 to 29 μW cm$^{-2}$ K$^{-2}$, with mode and median of 8.5 μW cm$^{-2}$ K$^{-2}$.

The thermal impedance of each TE generator could also be measured using the "hot strip" method [23]. The total thermal impedance $\Theta_{tot} = \Delta T/Q$, where $Q$ is the heat flow through the TEG under open-circuit conditions. Here, $Q = V_{heater}\cdot I_{heater}$, which is known from the bias applied to the heater resistor. Figure 3 shows $\Delta T$ vs. $Q$. The linear relationship has a slope that gives $\Theta_{tot} = 613.4$ K/W, including all parasitic series and leakage thermal impedances. Among all TE generator devices measured, $\Theta_{tot}$ ranged from 300 to 1200 K/W with most types having $\Theta_{tot}$ between 500 to 600 K/W.

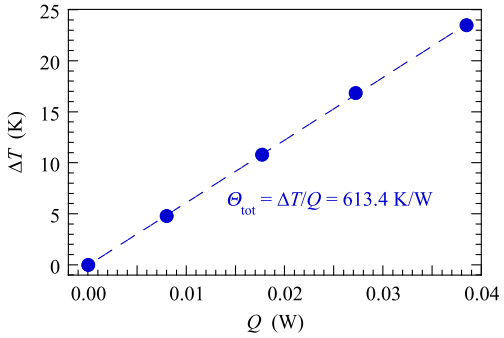


**Fig. 3** Measured temperature difference $\Delta T$ from resistive heater to chuck, plotted against heat flow $Q$ from the resistive heater. $Q$ is the product of the voltage and current biases applied to the heater. The dashed line is a linear least squares fit to the data. The slope of the line gives the total thermal impedance $\Theta_{tot} = 613.4$ K/*W* of the device

## 3 Performance Analysis

From thermal impedance measurements such as in Fig. 3 and knowledge of the device geometry and thermal conductivities of the materials used, we can reasonably estimate the temperature at the top of the Si nanoblade thermopile, $T_{H,TP}$, and the temperature at the bottom of the Si thermopile, $T_{C,TP}$, as opposed to the measured temperatures $T_H$ and $T_C$. Because of parasitic thermal impedances between the heater and the top of the thermopile and between the bottom of the thermopile and the chuck, the actual temperature difference across the thermopile itself, $\Delta T_{TP} = T_{H,TP} - T_{C,TP}$, is less than the applied temperature difference $\Delta T = T_H - T_C$. For most of our TE generators, our modeling shows that $\Delta T_{TP} \approx 0.1\ \Delta T$, i.e., for an applied $\Delta T$ of 20 K as measured by the thermometers in the heater and the chuck, the temperature difference across the thermopile itself is typically close to $\Delta T_{TP} \approx 2$ K.

Obtaining a reasonable estimate of $T_{H,TP}$ and $T_{C,TP}$ allows estimation of the *ZT* value of the Si nanoblades using the

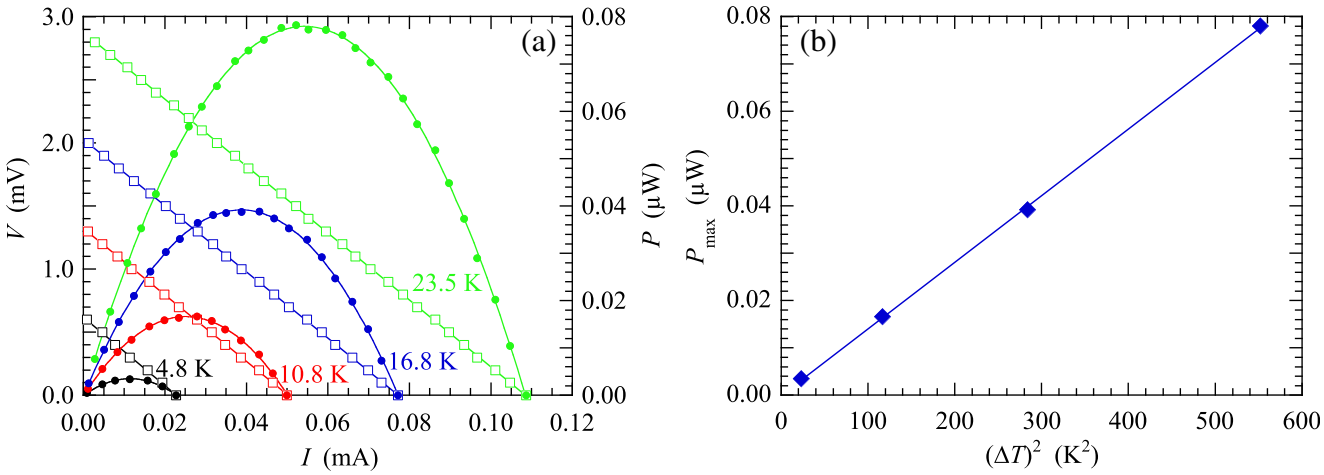


**Fig. 2** **a** Voltage (*V*, open squares) and power ($P = V \times I$, solid circles) vs. current (*I*) at $\Delta T = 4.8$ K (black), 10.8 K (red), 16.8 K (blue), and 23.5 K (green) for a representative TE generator. The curves are linear (for *V–I*) and quadratic (for *P–I*) least squares fits to the data. **b** Maximum power $P_{max} = \frac{1}{4}V_{OC}I_{SC}$ vs. $(\Delta T)^2$ from the data in (**a**). The solid line is a linear least squares fit

theoretical efficiency for a matched load $R_L = R_S$ [3], where $t = T_{C,\mathrm{TP}}/T_{H,\mathrm{TP}}$ is the temperature ratio between the top and bottom of the thermopile:

$$\frac{P_{\max}}{Q_H} = (1-t)\left(\frac{2ZT}{4(1+t)}\right)\left[1+ZT\left(\frac{5-t}{4(1+t)}\right)\right]^{-1} \quad (1)$$

The leading term (1–$t$) is the Carnot efficiency. Using Eq. 1 with the empirically determined $P_{\max}$ and $Q_{\mathrm{H}}$ and modeled value of $t$, we estimate the Si nanoblades in the TE generator whose characteristics are shown in Fig. 2 have $ZT \approx 0.007$, which is the same order-of-magnitude as bulk crystalline Si having similar dopant density [1, 2].

It appears paradoxical that the Si IC TE generators we developed have $\Gamma_P$ equal to that of the best high $ZT$ TE generators yet still have poor thermopile efficiency. The resolution lies in the fact that advanced Si processing can fabricate a far higher areal density of thermocouples than any competing material technology. Our Si TE generators typically have $> 4 \times 10^6$ thermocouples cm$^{-2}$. This is to be compared to the most advanced (Bi,Sb,Pb)(Te,Se) TE generators which have thermocouple densities $< 10^4$ cm$^{-2}$. Thus, the lower $ZT$ and hence efficiency of each Si nanoblade thermocouple can be compensated for by using more thermocouples per unit area to harvest heat.

## 4 Summary

In summary, the original work done by Ted Geballe and collaborators some 60 years ago showed the crystalline-doped Si should not be a practically useful thermoelectric material, prompting a decades long and continuing search for better TE materials. A half-century after their work, it was shown that crystalline Si in nanowire form could possibly be a useful TE material, but this promise was never fulfilled in any actual TE device. Our work demonstrates that, at least in certain microelectronic applications, integrated circuit Si TE generators can generate at least as much power per unit area per applied temperature difference as more exotic TE material technologies. The power generation performance out of Si IC TE generators comes not from an increase in TE figure-of-merit of nanostructure Si but from the ability of modern Si processing technology to fabricate a larger number of thermocouples per unit area to harvest heat and to control thermal and electrical parasitic impedances. Because our Si TE generators were made using standard industrial processes, it is straightforward to manufacture them in a commercially scalable manner at very low marginal cost.

**Acknowledgments** ML thanks Gangyi Hu and Hal Edwards for collaborating on this work.

**Funding Information** Work at UTD was sponsored by the National Science Foundation under contract ECCS-1707581.

## References

1. Geballe, T.H., Hull, G.W.: Seebeck effect in silicon. Phys. Rev. **98**, 940–947 (1955). https://doi.org/10.1103/PhysRev.98.940
2. Carruthers, J.A., Geballe, T.H., Rosenberg, H.M., Ziman, J.M.: The thermal conductivity of germanium and silicon between 2 and 300° K. Proc. R. Soc. A. **238**, 502–514 (1957). https://doi.org/10.1098/rspa.1957.0014
3. Tian, Z., Lee, S., Chen, G.: Comprehensive review of heat transfer in thermoelectric materials and devices. Annu. Rev. Heat Transf. **17**, 425–483 (2014). https://doi.org/10.1615/AnnualRevHeatTransfer.2014006932
4. Bell, L.E.: Cooling, heating, generating power, and recovering waste heat with thermoelectric systems. Science. **321**, 1457–1461 (2016). https://doi.org/10.1126/science.1158899]
5. Kraemer, D., Poudel, B., Feng, H.-P., Caylor, J.C., Yu, B., Yan, X., Ma, Y., Wang, X., Wang, D., Muto, A., McEnaney, K., Chiesa, M., Ren, Z., Chen, G.: High-performance flat-panel solar thermoelectric generators with high thermal concentration. Nat. Mater. **10**, 532–538 (2011). https://doi.org/10.1038/nmat3013
6. Chowdhury, I., Prasher, R., Lofgreen, K., Chrysler, G., Narasimhan, S., Mahajan, R., Koester, D., Alley, R., Venkatasubramanian, R.: On-chip cooling by superlattice-based thin-film thermoelectrics. Nat. Nanotech. **4**, 235–238 (2009). https://doi.org/10.1038/nnano.2008.417
7. Li, G., Fernandez, J.G., Ramos, D.A.L., Barati, V., Pérez, N., Soldatov, I., Reith, H., Schierning, G., Nielsch, K.: Integrated microthermoelectric coolers with rapid response time and high device reliability. Nat. Electron. **1**, 555–561 (2018). https://doi.org/10.1038/s41928-018-0148-3
8. Vullers, R.J.M., van Schaijk, R., Doms, I., Van Hoof, C., Mertens, R.: Micropower energy harvesting. Solid State Electron. **53**, 684–693 (2009). https://doi.org/10.1016/j.sse.2008.12.011
9. Hochbaum, A.I., Chen, R., Diaz Delgado, R., Liang, W., Garnett, E.C., Najarian, M., Majumdar, A., Yang, P.: Enhanced thermoelectric performance of rough silicon nanowires. Nature. **451**, 163–167 (2008). https://doi.org/10.1038/nature06381
10. Boukai, A.I., Bunimovich, Y., Tahir-Kheli, J., Yu, J.-K., Goddard, W.A., Heath, J.R.: Silicon nanowires as efficient thermoelectric materials. Nature. **451**, 168–171 (2008). https://doi.org/10.1038/nature06458
11. Oh, J.H., Shin, M., Jang, M.G.: Phonon thermal conductivity in silicon nanowires: the effects of surface roughness at low temperatures. J. Appl. Phys. **111**, 044304 (2012). https://doi.org/10.1063/1.3684973
12. Shi, L., Yao, D., Zhang, G., Li, B.: Size dependent thermoelectric properties of silicon nanowires. Appl. Phys. Lett. **95**, 063102 (2009). https://doi.org/10.1063/1.3204005
13. Zhang, G., Zhang, Q., Bui, C.-T., Lo, G.-Q., Li, B.: Thermoelectric performance of silicon nanowires. Appl. Phys. Lett. **94**, 213108 (2009). https://doi.org/10.1063/1.3143616
14. Zianni, X.: Monte Carlo simulations on the thermoelectric transport properties of width-modulated nanowires. J. Electron. Mater. **45**, 1779–1785 (2016). https://doi.org/10.1007/s11664-015-4217-3
15. Tomita, M., Oba, S., Himeda, Y., Yamato, R., Shima, K., Kumada, T., Xu, M., Takezawa, H., Mesaki, K., Tsuda, K., Hashimoto, S., Zhan, T., Zhang, H., Kamakura, Y., Suzuki, Y., Inokawa, H., Ikeda, H., Matsukawa, T.: Modeling, simulation, fabrication, and characterization of a 10-μW/cm$^2$ class Si-nanowire thermoelectric generator for IoT applications. IEEE Trans Elec. Dev. **65**, 5180–5188 (2018). https://doi.org/10.1109/ted.2018.2867845

16. Li, Y., Buddharaju, K., Singh, N., Lo, G.Q., Lee, S.J.: Chip-level thermoelectric power generators based on high-density silicon nanowire array prepared with top-down CMOS technology. IEEE Elec. Dev. Lett. **32**, 674–676 (2011). https://doi.org/10.1109/LED.2011.2114634
17. Dávila, D., Tarancón, A., Calaza, C., Salleras, M., Fernández-Regúlez, M., San Paulo, A., Fonseca, L.: Monolithically integrated thermoelectric energy harvester based on silicon nanowire arrays for powering micro/nanodevices. Nano Energy. **1**, 812–819 (2012). https://doi.org/10.1016/j.nanoen.2012.06.006
18. Curtin, B.M., Fang, E.W., Bowers, J.E.: Highly ordered vertical silicon nanowire array composite thin films for thermoelectric devices. J. Electron. Mater. **41**, 887–894 (2012). https://doi.org/10.1007/s11664-012-1904-1
19. Xie, J., Lee, C., Feng, H.: Design, fabrication, and characterization of CMOS MEMS-based thermoelectric power generators. J. Microelectromech. Syst. **19**, 317–324 (2010). https://doi.org/10.1109/JMEMS.2010.2041035
20. Yu, X., Wang, Y., Liu, Y., Li, T., Zhou, H., Gao, X., Feng, F., Roinila, T., Wang, Y.: CMOS MEMS-based thermoelectric generator with an efficient heat dissipation path. J. Micromech. Microeng. **22**, 105011 (2012). https://doi.org/10.1088/0960-1317/22/10/105011
21. Glatz, W., Schwyter, E., Durrer, L., Hierold, C.: $Bi_2Te_3$-based flexible micro thermoelectric generator with optimized design. J. Microelectromech. Syst. **18**, 763–772 (2009). https://doi.org/10.1109/JMEMS.2009.2021104]
22. Hu, G., Edwards, H., Lee, M.: Silicon integrated circuit thermoelectric generators with a high specific power generation capacity. Nat. Electron. **2**, 300–306 (2019). https://doi.org/10.1038/s41928-019-0271-9
23. Gustafsson, S., Karawacki, E., Khan, M.: Transient hot-strip method for simultaneously measuring thermal conductivity and thermal diffusivity of solids and fluids. J. Phys. D Appl. Phys. **12**, 1411–1421 (1979). https://doi.org/10.1088/0022-3727/12/9/003